JOURNAL OF AIRCRAFT
Vol. 40, No. 2, March–April 2003

Flow Angle, Temperature, and Aerodynamic Damping on Supersonic Panel Flutter Stability Boundary

Guangfeng Cheng*
Old Dominion University, Norfolk, Virginia 23529-0247
Y. Y. Lee†
City University of Hong Kong, Kowloon, Hong Kong, People's Republic of China
and
Chuh Mei‡
Old Dominion University, Norfolk, Virginia 23529-0247

The effects of flow yaw angle, temperature, and aerodynamic damping on supersonic flutter of plates are investigated. Quasisteady, first-order piston theory is employed for formulation of aerodynamic forces. The von Karman large-deflection plate theory is adapted for the aerothermal deflection. Two types of thermal effects are considered: 1) plate expansion by uniform temperature and 2) thermal moment induced by temperature gradient across the plate thickness. A finite element modal formulation and a two-step procedure are presented for the predictions of stability boundaries and nonlinear aerothermal deflection and shown to be efficient in solution. Results have shown that flow angle has lesser effect on stability boundaries as compared with temperature for isotropic square plates. However, both flow angle and temperature have a large influence on stability boundaries for rectangular isotropic and laminated composite plates. The presence of the "ripple" characteristics of stability boundaries for composite plates caused by the frequency coalescence of higher modes and the smaller effect of aerodynamic damping is investigated. The stabilization effects on panel motions induced by variations of flow angle, temperature, and aerodynamic damping are discussed.

Nomenclature

$[A_a]$, $[A_x]$, $[A_y]$	=	aerodynamic influence matrices
C_a	=	aerodynamic damping coefficient
$[G]$	=	aerodynamic damping matrix
g_a	=	nondimensional aerodynamic damping
h	=	plate thickness
$[K]$	=	stiffness matrix
$[M]$	=	mass matrix
$[N1]$, $[N2]$	=	first- and second-order incremental stiffness matrices
p_a	=	aerodynamic pressure
q_a	=	dynamic pressure
T_0, T_1	=	average temperature and temperature gradient across thickness
$\{W\}$	=	displacement vector in structure nodal degrees of freedom
β	=	$\sqrt{M_\infty^2 - 1}$
Λ	=	flow yaw angle
λ	=	nondimensional dynamic pressure
μ	=	nondimensional mass ratio
ρ	=	plate mass density
ρ_a	=	air mass density
ω_0	=	reference frequency

Subscripts

a	=	aerodynamic
b	=	bending
cr	=	critical
m	=	membrane
mb, bm	=	membrane/bending coupling
s	=	static
t	=	time dependent
x, y	=	coordinates x, y
ΔT	=	thermal

Received 19 July 2001; revision received 19 March 2002; accepted for publication 13 May 2002.

*Graduate Student, Aerospace Engineering Department. Student Member AIAA.
†Assistant Professor, Department of Building and Construction.
‡Professor, Aerospace Engineering Department. Associate Fellow AIAA.

Introduction

SURFACE panels of aerospace vehicles are subjected to supersonic/hypersonic airflow and thermal loads simultaneously. Such a complicated working environment might give rise to the dynamically instable phenomena of panel flutter, which contributes to structural fatigue failure.

The influence of arbitrary flow angle shown in Fig. 1 on the critical flutter dynamic pressure of isotropic and orthotropic rectangular panels with simply supported boundary conditions was studied analytically by Korders and Noll[1] and Bohon.[2] Durvasula[3,4] investigated the effects of flow angle and plate obliquity on the critical dynamic pressure of simply supported and clamped isotropic panels using the Rayleigh–Ritz method and 16-term beam functions. Early applications[5,6] of the finite element method (FEM) to the effects of flow angle on flutter were focused mainly on isotropic parallelogram panels. An excellent review of the FEM applied to linear models of supersonic aeroelastic stability analysis of plates and shells was given by Bismarck-Nasr.[7] Review of linear and nonlinear panel flutter analysis using various analytical methods including FEM was recently given by Mei et al.[8] Experiments[9,10] showed that orthotropic panels mounted on flexible supports experience large reductions in critical flutter dynamic pressure for only small changes in flow angle.

Few investigations of panel flutter have dealt directly with thermal effects. Houboult[11] was the first to study the thermal buckling stability and flutter boundary for two-dimensional plates subjected to uniform temperature distribution. Yang and Han[12] studied the linear flutter of thermally buckled two-dimensional panels using FEM. More recent research has extended to nonlinear flutter of

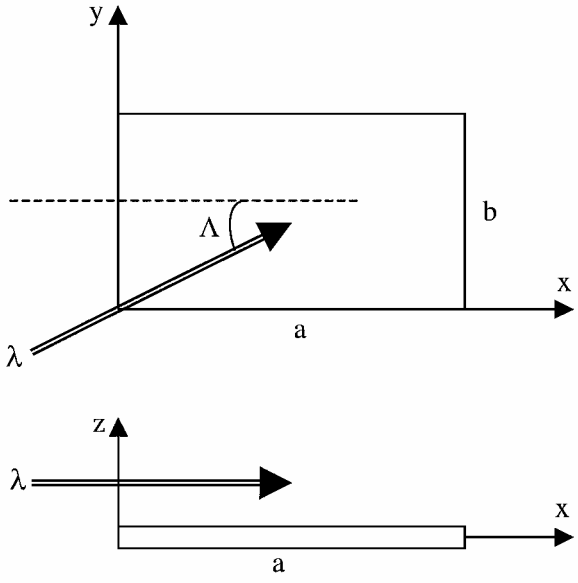

Fig. 1 Sketch of plate geometry.

panels under various temperature distributions. Xue and Mei[13,14] investigated the flutter boundaries of thermally buckled plates under nonuniform temperature distributions using FEM and von Karman large-deflection plate theory for structural nonlinearity. Liaw[15] included geometrical nonlinearities in finite element formulation and studied supersonic flutter of laminated composite plates.

The flutter characteristics of laminated composite panels at various flow angles in supersonic flow and at elevated temperatures had not been discussed in the literature. Kariappa et al.[5] treated the thermal loads as in-plane forces (less than the buckling load) and investigated the effects of yawing angles and inplane forces on supersonic flutter of skewed panels using FEM. Their studies were limited to: 1) linear aerodynamic models and linear structures, 2) isotropic plates, and 3) no bending moment effects caused by temperature gradient across plate thickness.

The present paper examines the supersonic panel flutter characteristics of isotropic and laminated composite plates using FEM considering both flow angularity and temperature effects. Both the finite element system equations in structure nodal degrees of freedom and the solution procedure developed by Xue and Mei[13] are extended to include flow angle and temperature gradient effects. The modal reduction technique has been shown to be efficient in various types of flutter analysis.[16–18] Modal transformation is applied here to reduce the total number of equations to save computation costs yet maintain acceptable accuracies. The nonlinear modal equations for static aerothermal deflection induced by thermal expansion/bending and aerodynamic pressure are solved numerically by using the Newton–Raphson method. Flutter boundaries are determined through eigenanalysis of dynamic motion of plate about the deformed plate configuration. An isotropic plate and a symmetrically laminated plate are used as examples. Results showed that flow angle and temperature have great influence on stability boundaries of laminated composite and isotropic rectangular plates. The discovery of the "ripple" characteristics of stability boundaries for the composite plates, which is believed to be the first time, is investigated and discussed in detail. The stability boundaries of composite plate at various flow yaw angles and at combined uniform temperature and thickness temperature gradient distributions are obtained for the first time in the literature.

Finite Element Formulation

System Equations of Motion

With both aerodynamic pressure and thermal loads the plate will experience large-amplitude nonlinear response as flow speed and/or temperature increased to a certain high level. To address this influence from nonlinear plate response, the contributions from nonlinear inplane strain components according to von Karman large-deflection theory are taken into account.

The thermal effect can be considered by including the thermal stress resultants $\{N_{\Delta T}\}$ and $\{M_{\Delta T}\}$, which are the thermal force and thermal moment induced by the change of temperature, respectively. For thin-walled structures that have extensive applications in aircraft, the close to reality steady-state temperature field is a function of all three coordinates, that is, $\Delta T(x, y, z)$. As suggested by some earlier researchers,[19,20] the temperature variation can be assumed to be linearly distributed across the plate thickness as $\Delta T = T_0 + zT_1/h$. By setting $T_1 = 0.0$, a special case of uniform temperature distribution is reached.

The present work falls into the type 3 analysis categorized by Dowell.[21] That is, linear quasisteady aerodynamic theory is employed to model the pressure fluctuation over the vibrating plate. Among the aerodynamic theories approximating unsteady airflow with quasisteady flow field, the family of piston theories[22] was proved to be a useful tool to flutter analysis. The linear quasisteady first-order piston theory, if flow angle is denoted as Λ, is given as

$$p_a = -\frac{2q_a}{\beta}\left[\left(\frac{M_\infty^2 - 2}{M_\infty^2 - 1}\right)\frac{1}{V_\infty}w_{,t} + w_{,x}\cos\Lambda + w_{,y}\sin\Lambda\right]$$

$$= -\frac{g_a}{\omega_0}\frac{D_{110}}{a^4}w_{,t} - \lambda\frac{D_{110}}{a^3}w_{,x}\cos\Lambda - \lambda\frac{D_{110}}{a^3}w_{,y}\sin\Lambda \qquad (1)$$

where $q_a = \rho_a V_\infty^2/2$ is the dynamic pressure, $\beta = \sqrt{M_\infty^2 - 1}$, D_{110} is the first entry of laminate bending rigidity $[D]$ for a unidirectional zero-degree laminate, and a is the length of the rectangular plate. The nondimensional dynamic pressure λ and aerodynamic damping g_a are defined as

$$\lambda = 2q_a a^3 \big/ \beta D_{110}, \qquad g_a = \sqrt{\lambda C_a} \qquad (2)$$

where aerodynamic damping $C_a = \mu(M_\infty^2 - 2)^2/\beta(M_\infty^2 - 1)^2$ and mass ratio $\mu = \rho_a a/\rho h$. For $M_\infty \gg 1$, $C_a \approx \mu/M_\infty$.

The system equations of motion can be derived from the principle of virtual work, with internal energy accumulated through stress resultants and external work done by aerodynamic pressure and inertia force. After assembling the element matrices and applying the boundary conditions, the equations governing the panel motion can be expressed as described by Xue and Mei[14] and Abdel-Motaglay et al.[16]

$$\frac{1}{\omega_0^2}\begin{bmatrix}[M_b] & 0\\ 0 & [M_m]\end{bmatrix}\begin{Bmatrix}\ddot{W}_b\\ \ddot{W}_m\end{Bmatrix} + \frac{g_a}{\omega_0}\begin{bmatrix}[G] & 0\\ 0 & 0\end{bmatrix}\begin{Bmatrix}\dot{W}_b\\ \dot{W}_m\end{Bmatrix}$$

$$+\left(\lambda\begin{bmatrix}[A_x]\cos\Lambda + [A_y]\sin\Lambda & 0\\ 0 & 0\end{bmatrix} + \begin{bmatrix}K_b & K_{\mathrm{bm}}\\ K_{\mathrm{mb}} & K_m\end{bmatrix}\right.$$

$$-\begin{bmatrix}K_{N\Delta T} & 0\\ 0 & 0\end{bmatrix} + \frac{1}{2}\begin{bmatrix}[N1_{\mathrm{Nm}}] + [N1_{\mathrm{NB}}] & [N1_{\mathrm{bm}}]\\ [N1_{\mathrm{mb}}] & 0\end{bmatrix}$$

$$\left.+\frac{1}{3}\begin{bmatrix}[N2] & 0\\ 0 & 0\end{bmatrix}\right)\begin{Bmatrix}W_b\\ W_m\end{Bmatrix} = \begin{Bmatrix}P_{b\Delta T}\\ P_{m\Delta T}\end{Bmatrix}$$

or

$$\left(1/\omega_0^2\right)[M]\{\ddot{W}\} + (g_a/\omega_0)[G]\{\dot{W}\} + \left(\lambda[A_a] + [K] - [K_{N\Delta T}]\right.$$

$$\left.+\tfrac{1}{2}[N1] + \tfrac{1}{3}[N2]\right)\{W\} = \{P_{\Delta T}\} \qquad (3)$$

where $\omega_0 = (D_{110}/\rho h a^4)^{1/2}$ is a reference frequency. The flow angle effect is introduced in the aerodynamic influence matrix $[A_a] = [A_x]\cos\Lambda + [A_y]\sin\Lambda$. Temperature is induced in the linear geometrical stiffness matrix $[K_{N\Delta T}]$ as a result of thermal stress resultant $\{N_{\Delta T}\}$ and in the thermal load vector $\{P_{\Delta T}\}$. And $[N1]$ and $[N2]$ are the first- and second-order nonlinear stiffness matrices caused by large deflections, respectively. For isotropic or symmetrically laminated composite plates, Eq. (3) can be simplified because $[K_{\mathrm{bm}}]$, $[K_{\mathrm{mb}}]$, and $[N1_{\mathrm{NB}}]$ are zero and $\{P_{b\Delta T}\}$ is zero for the uniformly distributed temperature case.

Solution Procedure

To determine the flutter boundary, the solution of Eq. (3) can be assumed as

$$\{W\} = \{W\}_s + \{W\}_t \tag{4}$$

where $\{W\}_s$ is the aerothermal deflection (particular solution) caused by aerodynamic pressure and thermal loads and $\{W\}_t$ is the small oscillations of the plate about the aerothermally deformed equilibrium position (homogeneous solution). Therefore, $\{W\}_s$ is treated as a quasi-static deflection of the plate and is time independent, while $\{W\}_t$ is the dynamic response of the plate. Consequently, the solution procedure contains two steps corresponding to the determination of $\{W\}_s$ and $\{W\}_t$, respectively.

As an intrinsic characteristic of flutter, occurrence of frequency coalescence between different modes of plate vibration can be utilized to mark the flutter boundary. Once flutter starts, the plate motion can be limit-cycle oscillations (LCO), periodic but not simple harmonic motion, nonperiodic motion, or chaotic motion.[18,23] However, at the vicinity of flutter boundary the amplitude of vibration is quite small. Therefore, it is reasonable to assume $\{W\}_t \ll \{W\}_s$ immediately after the commencement of flutter. Observing this relationship, by substitution of Eq. (4) into Eq. (3) and neglecting the higher order terms of $\{W\}_t$, Eq. (3) can be separated into two equations:

$$\left(\lambda[A_a] + [K] - [K_{N\Delta T}] + \tfrac{1}{2}[N1]_s + \tfrac{1}{3}[N2]_s\right)\{W\}_s = \{P_{\Delta T}\} \tag{5}$$

and

$$\left(1/\omega_0^2\right)[M]\{\ddot{W}\}_t + (g_a/\omega_0)[G]\{\dot{W}\}_t + (\lambda[A_a] + [K] - [K_{N\Delta T}] + [N1]_s + [N2]_s)\{W\}_t = 0 \tag{6}$$

where the subscript s on $[N1]$ and $[N2]$ denotes that they are evaluated with the aerothermal deflection $\{W\}_s$. Mathematically, these two equations are solved for the particular $\{W\}_s$ and homogeneous $\{W\}_t$ solutions of the original nonhomogeneous partial differential equation. They are equivalent to Eq. (3) only under the assumption of small dynamic responses. If the plate has large-amplitude dynamic motion, nonlinear stiffness contributions from the dynamic deflection $\{W\}_t$ must be included as described by Xue and Mei.[14]

For the plate with a uniform temperature distribution, its motion is characterized by dynamic pressure λ as studied by Xue[24] (see Figs. 2a and 2b): 1) at temperatures lower than the critical buckling temperature, the plate is initially flat $\{W\}_s = 0$, and then undergoes LCO as $\lambda > \lambda_{cr}$; and 2) at temperatures beyond the thermal buckling temperature, the plate is initially buckled at small λ, and, subsequently, it becomes flat $\{W\}_s = 0$, at moderate λ until LCO or chaotic motion commences as $\lambda > \lambda_{cr}$. To take advantage of this knowledge, a linear model, formed with Eq. (6) in which $[N1]_s$ and $[N2]_s$ are zero, is employed to determine the flutter boundary for temperatures less than the critical buckling temperature. However, for the aerothermally buckled plate the set of nonlinear algebraic equations given in Eq. (5) must be solved first for postbuckling deflections, which are then used to evaluate $[N1]_s$ and $[N2]_s$ in Eq. (6). As the plate experiences a thermal moment induced by the temperature gradient, bending deflection as a result of thermal effects exists regardless of the dynamic pressure. A nonlinear equation solver is applied to determine the plate static equilibrium position, which is then used to evaluate the nonlinear stiffness matrices. All matrices in Eq. (6) are therefore known, and eigenanalysis is applied to trace the frequency coalescence. The flutter boundary is reached when the plate damping rate α becomes positive [see Eq. (22)] as well as frequency coalescence occurs.

Only isotropic and symmetrically laminated plates are studied in this paper; thus, the governing equations given in Eqs. (5) and (6) can be simplified. The bending-extension coupling matrix $[B]$ vanishes for either isotropic or symmetrically laminated plates. By neglecting the membrane inertia term in Eq. (6), the in-plane displacement vector can be expressed in terms of the bending displacement vectors as

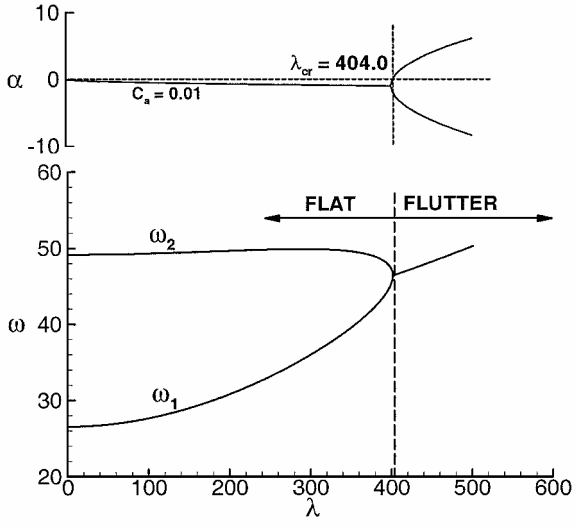

a) $T_0/\Delta T_{cr} < 1.0$

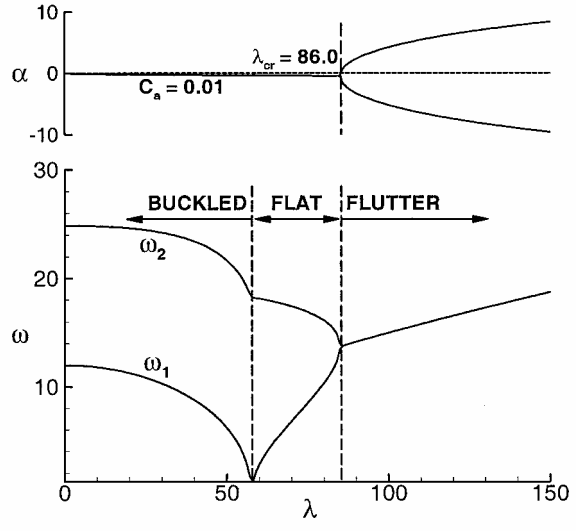

b) $T_0/\Delta T_{cr} = 1.1$

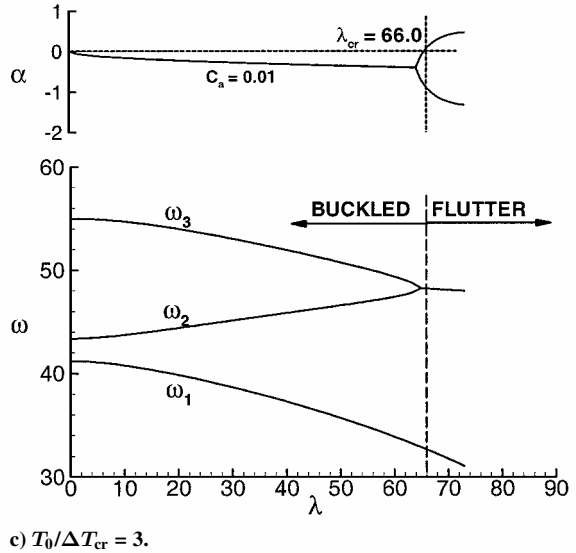

c) $T_0/\Delta T_{cr} = 3.$

Fig. 2 Frequency coalescence analysis of clamped $[0/45/-45/90]_s$ rectangular plate at $\Lambda = 45$ deg and uniform temperatures.

$$\{W_m\}_s = [K_m]^{-1}\left(\{P_{m\Delta T}\} - \tfrac{1}{2}[N1_{\rm mb}]_s\{W_b\}_s\right)$$

$$\{W_m\}_t = -[K_m]^{-1}[N1_{\rm mb}]_s\{W_m\}_t \tag{7}$$

Substituting Eq. (7) into Eqs. (5) and (6), the equations governing the static and dynamic bending of the plate are

$$\left(\lambda[A_a] + [K_b] - [K_{N\Delta T}] + \tfrac{1}{2}[N1_{\rm Nm}]_s + \tfrac{1}{3}[N2]_s - \tfrac{1}{4}[N1_{\rm bm}]_s[K_m]^{-1}[N1_{\rm mb}]_s\right)\{W_b\}_s + \tfrac{1}{2}[N1_{\rm bm}]_s[K_m]^{-1}\{P_{m\Delta T}\} = \{P_{b\Delta T}\} \tag{8}$$

$$\left(1/\omega_0^2\right)[M_b]\{\ddot{W}_b\}_t + (g_a/\omega_0)[G]\{\dot{W}_b\}_t + \left(\lambda[A_a] + [K_b] - [K_{N\Delta T}] + [N1_{\rm Nm}]_s - [N1_{\rm bm}]_s[K_m]^{-1}[N1_{\rm mb}]_s + [N2]_s\right)\{W_b\}_t = 0 \tag{9}$$

Critical Buckling Temperature

Thermal buckling only happens when isotropic or symmetrically laminated plates are heated uniformly. But for any plate acted by thermal moments, the plate will deform. For the latter case there is neither buckling phenomenon nor an associated critical buckling temperature. For the current study the critical buckling temperature is used as a reference for the case of a plate with thermal moments. The procedure to determine the critical buckling temperature can be found in related literature, such as Yang and Han[12] and Shi et al.[17] For an isotropic or symmetrically laminated plate heated uniformly, the critical buckling temperature is

$$\Delta T_{\rm cr} = \mu_1 T_0 \tag{10}$$

where μ_1 is the lowest eigenvalue of thermal buckling found from the eigenproblem

$$[K_b]\{\phi\} = \mu([K_{N\Delta T}] - [N1_{\rm Nm}])\{\phi\} \tag{11}$$

where $\{\phi\}$ is the corresponding buckling mode shape.

Aerothermal Deflection

The static plate deflection from aerodynamic pressure and temperature can be determined by solving the nonlinear equations given in Eq. (5) or Eq. (8) with a nonlinear equation solver. However, difficulties exist while trying to solve a large number of equilibrium equations, whether or not the plate is modeled with a moderately fine mesh size. This makes the root finding procedure quite time consuming. One solution to this difficulty is the use of modal coordinates, which is based upon the expansion theorem and modal reduction techniques.

The expansion theorem states that any possible motion of the system can be described as a linear combination of the modal vectors. And, the essence of modal reduction is to restrain the dominating modal contributions. Applying to the present flutter problem, an assumption resembling Eq. (4) becomes

$$\{W_b\} = \{W_b\}_s + \{W_b\}_t = \sum_{i=1}^{n} q_i\{\phi_i\} = \sum_{i=1}^{n}(q_{\rm si} + q_{\rm ti})\{\phi_i\} = [\Phi](\{q\}_s + \{q\}_t) \tag{12}$$

where q_{si} and $\{q\}_s$ represent modal coordinate coefficients for each mode participating in the static response and $q_{\rm ti}$ and $\{q\}_t$ are modal coordinate coefficients for dynamic response. The number of modes n used in the model is usually a small number. The modal matrix $[\Phi]$ consists of mode shapes of dominant modes. For the case of the uniform temperature distribution, if the temperature is below the critical buckling temperature $\Delta T_{\rm cr}$ linear vibration modes are used. Whereas, when the temperature increases beyond $\Delta T_{\rm cr}$, thermal buckling modes are used. For cases with a temperature gradient, linear vibration modes are used.

The modal equation for static bending of the plate is derived by substituting $\{W_b\}_s = [\Phi]\{q\}_s$ into Eq. (8) and premultiplication by $[\Phi]^T$ as follows:

$$[\Phi]^T\left(\lambda[A_a] + [K_b] - [K_{N\Delta T}] + \tfrac{1}{2}[N1_{\rm Nm}]_s + \tfrac{1}{3}[N2]_s - \tfrac{1}{4}[N1_{\rm bm}]_s[K_m]^{-1}[N1_{\rm mb}]_s\right)[\Phi]\{q\}_s + \tfrac{1}{2}[\Phi]^T[N1_{\rm bm}]_s[K_m]^{-1}\{P_{m\Delta T}\} = [\Phi]^T\{P_{b\Delta T}\} \tag{13}$$

The number of the nonlinear algebraic equations is reduced dramatically. Several nonlinear equation solvers exist that will determine the modal coordinates. Herein the Newton–Raphson iterative method is applied.

In Eq. (13) the nonlinear stiffness matrices can be evaluated with modal coordinates as

$$[N1_{\rm mb}]_s = \sum_{i=1}^{n} q_{\rm si}[N1_{\rm mb}]^{(i)}, \qquad [N2]_s = \sum_{i=1}^{n}\sum_{j=1}^{n} q_{\rm si}q_{\rm sj}[N2]^{(ij)} \tag{14a}$$

where the superscript i denotes that $\{\phi_i\}$ is used in evaluation of the first-order nonlinear modal stiffness matrix. Similarly, the superscript ij denotes that $\{\phi_i\}$ and $\{\phi_j\}$ are used in evaluation of the second-order nonlinear modal stiffness matrix. The nonlinear modal stiffness matrices $[N1_{\rm mb}]^{(i)}$ and $[N2]^{(ij)}$ are constant.

The matrix $[N1_{\rm Nm}]_s$ contains a constant part $[N1_{\rm Nm}]_0$ and a quadratic part $[N1_{\rm Nm}]_{s2}$, corresponding to the two terms of $\{W_m\}_s$ in Eq. (7). The constant $[N1_{\rm Nm}]_0$ is evaluated by the first term $\{W_m\}_0 = [K_m]^{-1}\{P_{m\Delta T}\}$, and the quadratic matrix $[N1_{\rm Nm}]_{s2}$ is

$$[N1_{\rm Nm}]_{s2} = \sum_{i=1}^{n}\sum_{j=1}^{n} q_{\rm si}q_{\rm sj}[N1_{\rm Nm}]_{s2}^{(ij)} \tag{14b}$$

where $[N1_{\rm Nm}]_{s2}^{(ij)}$ is evaluated with the second term $\{W_m\}_{s2}^{(ij)} = -\tfrac{1}{2}[K_m]^{-1}[N1_{\rm mb}]_s^{(i)}\{\phi_j\}$ and $[N1_{\rm Nm}]_{s2}^{(ij)}$ is a constant matrix.

With application of the Newton–Raphson method, the kth iteration step provides

$$[K_T]_k\{\Delta q\}_{s,k+1} = \{\Delta P\}_k \tag{15}$$

and

$$\{q\}_{s,k+1} = \{q\}_{s,k} + \{\Delta q\}_{s,k+1} \tag{16}$$

where the tangent stiffness matrix and unbalanced load vector are

$$[K_T]_k = [\Phi]^T\left(\lambda[A_a] + [K_b] - [K_{N\Delta T}] + \tfrac{1}{2}[N1_{\rm Nm}]_0 + [N1_{\rm Nm}]_{s2} + [N2]_s - [N1_{\rm bm}]_s[K_m]^{-1}[N1_{\rm mb}]_s\right)[\Phi] \tag{17}$$

$$\{\Delta P\}_k = [\Phi]^T\{P_{b\Delta T}\} - [\Phi]^T\left(\lambda[A_a] + [K_b] - [K_{N\Delta T}] + \tfrac{1}{2}[N1_{\rm Nm}]_0 + \tfrac{1}{2}[N1_{\rm Nm}]_{s2} + \tfrac{1}{3}[N2]_s - \tfrac{1}{4}[N1_{\rm bm}]_s[K_m]^{-1}[N1_{\rm mb}]_s\right)[\Phi]\{q\}_{sk} - \tfrac{1}{2}[\Phi]^T[N1_{\rm bm}]_s[K_m]^{-1}\{P_{m\Delta T}\} \tag{18}$$

Convergence is accepted when the absolute norm (see Ref. 25) of the $\{q\}_s$ is lower than 10^{-5}.

Stability Boundary

Having determined the static aerothermal deflection, the nonlinear stiffness matrices in Eq. (9) can be evaluated with this static deflection. Therefore, Eq. (9) is in fact a linear dynamic equation. Using the dynamic response given in Eq. (12), $\{W_b\}_t = [\Phi]\{q\}_t$, the dynamic equation of motion is transferred into modal coordinates

$$\left(1/\omega_0^2\right)[\bar{M}_b]\{\ddot{q}\}_t + (g_a/\omega_0)[\bar{G}]\{\dot{q}\}_t + [\bar{K}]\{q\}_t = 0 \tag{19}$$

where the modal mass, aerodynamic damping, and linear stiffness matrices are defined as

$$[\bar{M}_b] = [\Phi]^T[M_b][\Phi], \qquad [\bar{G}] = [\Phi]^T[G][\Phi]$$

$$[\bar{K}] = [\Phi]^T\big(\lambda[A_a] + [K_b] - [K_{N\Delta T}] + [N1_{\mathrm{Nm}}]_s - [N1_{\mathrm{bm}}]_s[K_m]^{-1}[N1_{\mathrm{mb}}]_s + [N2]_s\big)[\Phi] \tag{20}$$

The flutter boundary is determined from eigenanalysis of Eq. (19)

$$\kappa[\bar{M}_b]\{X\} = [\bar{K}]\{X\} \tag{21}$$

where the nondimensional eigenvalue κ is defined as

$$\kappa = -(\Omega/\omega_0)^2 - g_a(\Omega/\omega_0) \tag{22}$$

and where $\Omega = \alpha + i\omega$ in which α and ω are the panel damping rate and frequency, respectively. As the nondimensional dynamic pressure λ is increased, some system frequencies might coalesce. If α is found to be positive when coalescence exists, the motion of the plate is unstable. The corresponding value of λ is taken as the stability boundary λ_{cr} as α crossing from negative to positive (see Fig. 2).

Numerical Results and Discussions

The 24-degree-of-freedom Bogner–Fox–Schmit C^1 conforming rectangular plate element is used for the finite element model. Four specific flow angles, $\Lambda = 0$, 15, 30, and 45 deg, are selected to examine the stability characteristics. Taking ΔT_{cr} as the reference, the flutter boundaries at different temperature ratios $\Delta T/\Delta T_{\mathrm{cr}}$ are studied to investigate the effect of temperature and flow yaw angle on flutter boundaries.

Isotropic Plates

To verify the current finite element model and solution procedure, the flutter boundary of an isotropic plate is investigated. As modal formulation is employed in present work, an important issue is the selection of modes. Dowell[21,23] indicated that for the case of flow angle $\Lambda = 0$ deg, 6 linear modes, (1, 1), (2, 1) to (6, 1), give quite accurate results for LCO. However, more recent research has unveiled the complexity of mode selection. Weiliang and Dowell[26] found that more than one spanwise mode is required for sufficient analysis of LCO response for the cantilever isotropic plate. Lee et al.[27] encountered difficulty of tracking frequency coalescing modes when temperature effects are involved. They adopted a mode tracking scheme to follow modes that will coalesce. All of these studies indicate that the sequence of coalescing modes changes with different types of boundary conditions, aspect ratios, material properties, etc. In addition, if the temperature distribution is complex the possibility of new mode characteristics will make the coalescence of modes more complicated. Because spanwise modes are important for all flow angle cases and the composite plate possesses anisotropic material properties, herein an equal number of modes—modes (1, 1) to (n, n)—along the length and width of the plate is employed. To determine the number of modes to be used, modal convergence was studied and is shown in Table 1. It is observed that using 16 modes—mode (1, 1) to mode (4, 4)—will provide quite accurate flutter boundaries. Another issue for finite element analysis is the mesh size, which necessitates the mesh convergence study as summarized in Table 2. Results show that the 12×12 mesh should be used. Based upon the modal convergence and mesh convergence results, up to 16 modes and a 12×12 mesh are employed in present work.

Because the solution procedure contains two steps, the nonlinear equation solver and the eigenanalysis module are verified separately. Figure 3 compares results of thermal postbuckling deflections of a clamped isotropic plate from the current Newton–Raphson approach to those results of Paul[28] using an analytical method. The postbuckling deflection solver gives accurate predictions.

To illustrate the eigenanalysis procedure, the stability boundaries of a simply supported isotropic plate at four typical flow angles are shown in Fig. 4. Curve AD is the flutter stability boundary,

Table 1 Convergence of stability boundary λ_{cr} vs number of modes for a simply supported isotropic square plate (flow angle $\Lambda = 45$ deg)

	Number of modes			
$T_0/\Delta T_{\mathrm{cr}}$	4	9	16	25
0.0	439	539	523	527
1.5	242	273	270	271
3.0	199	210	208	208

Table 2 Convergence of stability boundary λ_{cr} vs mesh sizes for the simply supported isotropic square plate (flow angle $\Lambda = 45$ deg)

	Mesh sizes			
$T_0/\Delta T_{\mathrm{cr}}$	8×8	10×10	12×12	16×16
0.0	523	523	523	523
1.5	270	270	270	270
3.0	209	209	208	208

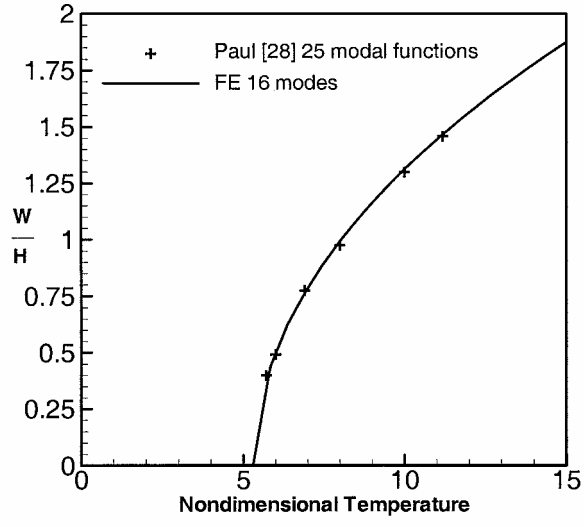

Fig. 3 Comparison of thermal postbuckling deflections for a clamped isotropic square plate.

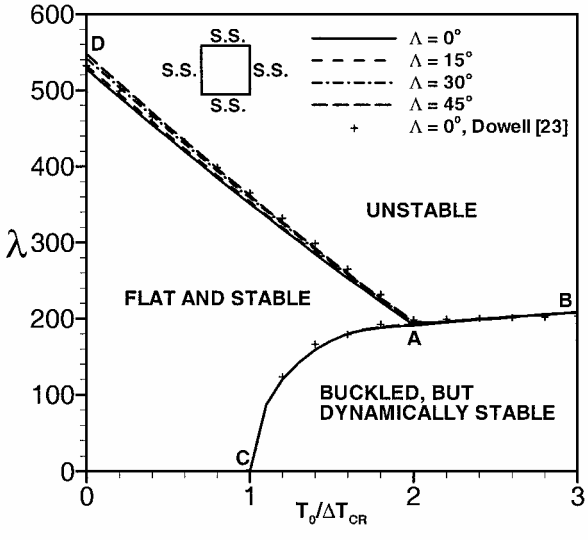

Fig. 4 Stability boundaries of simply supported square plate with uniform temperature and various flow angles ($C_a = 0.1$).

curve AC is the buckling stability boundary, and curve AB denotes the boundary from buckled but dynamically stable ($\{W\}_s \neq 0$, $\{W\}_t = 0$) plate to the unstable plate. Flutter boundaries ($\Lambda = 0$ deg only) from Dowell[23] are also given for comparison. Good agreement is obtained. Obviously, the flow angle brings little effect to stability boundaries for the simply supported square plate. However, as temperature is increased, the flutter stability boundary AD drops drastically, whereas stability boundary AB varies just slightly.

The analysis of isotropic plates illustrates the finite element modal procedure, and it is observed that for isotropic square plates the variation of the stability boundaries caused by changes of flow angle and elevated temperature is dominated by the latter. However, it is anticipated that for rectangular plates, as studied by Durvasula[3,4] using analytical methods and by Abdel-Motaglay et al.[16] using FEM, changes of the flow angle will cause a significant variation of the stability boundaries. A study of rectangular composite plates is conducted to confirm this behavior.

Composite Plates

The stability boundaries of a rectangular composite plate are investigated in this section. The plate is an eight-layer $[0/45/-45/90]_s$ graphite/epoxy laminate with dimensions of $38.1 \times 30.5 \times 0.122$ cm ($15 \times 12 \times 0.048$ in.). The material properties are

$$E_1 = 155 \text{ MPa (22.5 Msi)}, \qquad E_2 = 8.07 \text{ GPa (1.17 Msi)}$$

$$G_{12} = 4.55 \text{ GPa (0.66 Msi)}, \qquad \nu_{12} = 0.22$$

$$\alpha_1 = -0.07 \times 10^{-6}/^\circ\text{C}(-0.04 \times 10^{-6}/^\circ F)$$

$$\alpha_2 = 30.1 \times 10^{-6}/^\circ\text{C}(16.7 \times 10^{-6}/^\circ\text{F})$$

$$\rho = 1550 \text{ kg/m}^3(0.1458 \times 10^{-3} \text{ lb} - \text{s}^2/\text{in}^4.)$$

Flutter of Plates with Uniform Temperatures

The flutter boundaries of a composite plate with all edges clamped are studied first. Figure 5 shows the stability boundaries with flow angles $\Lambda = 0$, 15, 30, and 45 deg and temperature ratios $T_0/\Delta T_{cr}$ ($\Delta T_{cr} = 36.471^\circ$F or 20.26°C) from 0.0 to 3.0. As found with isotropic plates, the plate behavior may be flat and stable ($\{W\}_s = 0$, $\{W\}_t = 0$), buckled but dynamically stable ($\{W\}_s \neq 0$, $\{W\}_t = 0$), or unstable as shown in Fig. 5. And, increases of temperature result in stability boundary changes similar to isotropic plates. However, there are three issues that must be addressed.

The first issue is concerned with the destabilization, or stabilization, effects caused by nonzero flow angle. In Fig. 5, it is seen that

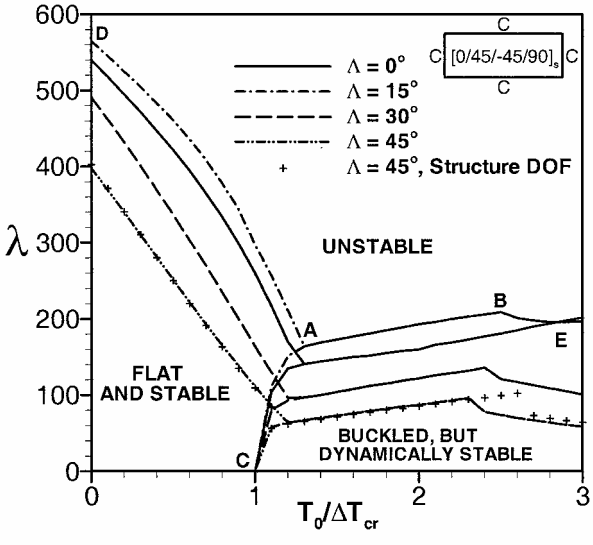

Fig. 5 Stability boundaries of a clamped $[0/45/-45/90]_s$ rectangular plate with uniform temperature and various flow angles ($C_a = 0.01$).

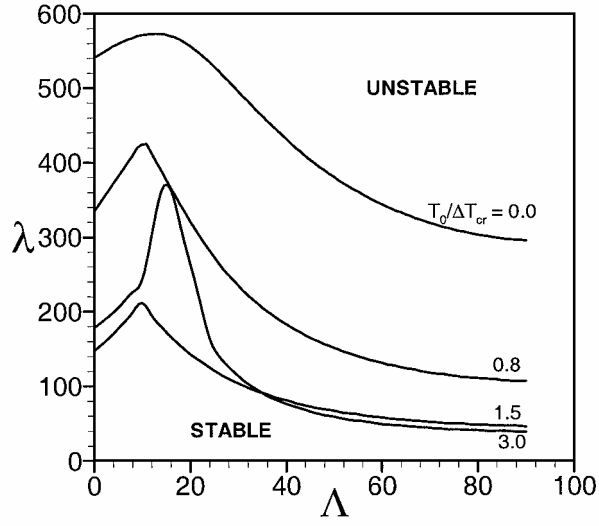

Fig. 6 Stability boundary variation vs flow angle for a clamped $[0/45/-45/90]_s$ rectangular plate at uniform temperatures ($C_a = 0.01$).

the change of flow angle affects the stability boundaries greatly for the composite as compared to the isotropic plates (Fig. 4). Increases of flow angle is observed to enhance stability. But at high flow angles a decrease of stability boundary is observed. To study the flow angle effects in detail, the variation of stability boundary with respect to continuous change of flow angles for several temperature ratios is investigated. Figure 6 shows the variations of λ at different temperature ratios. There exists an optimum flow angle, and its value falls into the range of 5 to 20 deg. The destabilization magnitude beyond this optimum angle is notable. For design purposes the case of the large flow angle is of concern. However, different results occur as changes in the aspect ratio, boundary conditions, material properties and/or laminate stacking sequence varied, as investigated by Durvasula[4] using the Galerkin method.

The second issue is the abrupt drop of the stability boundary at high temperature ratios and nonzero flow angle. With comparison of stability boundaries depicted in Fig. 5 with those given in Fig. 4 for the isotropic plate, it is shown that there is the decreasing curve BE for nonzero flow angle cases. In Fig. 5, the results from analysis using Eq. (9) in the structure degrees-of-freedom approach confirm this phenomenon; this concludes that the ripple is not attributed to the smaller number of system equations of the modal method. The explanation to the appearance of this ripple can be inferred from the frequency coalescence analysis for the case of flow angle $\Lambda = 45$ deg given in detail in Fig. 2. Coalescence behavior described in Fig. 2a is the typical eigenvalue coalescence form of linear models. This approach is a standard method for seeking the stability boundary of an unbuckled plate, for example, plate with $T_0/\Delta T_{cr} < 1.0$. Figure 2b traces the eigenvalue variations of the buckled plate at $T_0/\Delta T_{cr} = 1.1$. Figure 2c shows that at the high temperature ratio $T_0/\Delta T_{cr} = 3.0$ the thermally buckled plate will flutter and result in a lower stability boundary. The coalescence modes in Fig. 2c are different from those in Figs. 2a and 2b. For a physical understanding the high temperature and the anisotropic characteristics of composites and the flow direction to the chord can lead to a frequency coalescence between modes other than the lowest two modes as well as a reduction in the stability boundary. The stability curve for the composite plate at nonzero flow angles shown in Fig. 5 consist of three sections: curve AD is the flutter boundary, curve AC is the buckling boundary, curve ABE is the buckling to flutter boundary.

The third issue evoked by observation of Fig. 5 is the influence of aerodynamic damping. Aerodynamic damping of $C_a = 0.01$ is used in the response curves in Fig. 5. Some researchers have ignored aerodynamic damping ($C_a = 0.0$) in their analyses. It appears that the ripples might be related to the aerodynamic damping applied. According to Dowell,[21] the typical aerodynamic damping ranges from $C_a = 0.01$ to 0.1. Further efforts are necessary to investigate

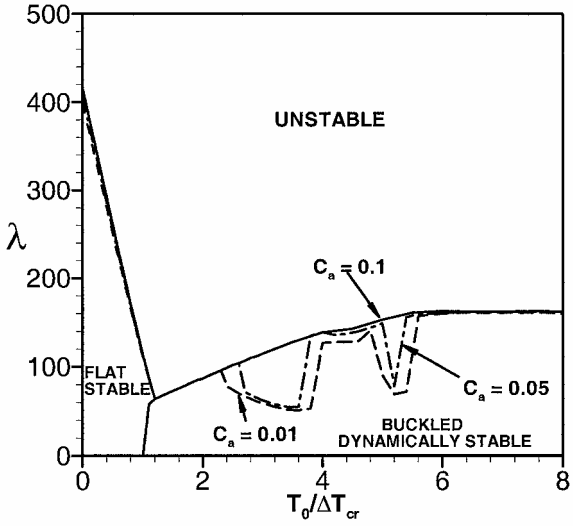

Fig. 7 Aerodynamic damping effect for clamped [0/45/−45/90]$_s$ rectangular plate; Λ = 45 deg.

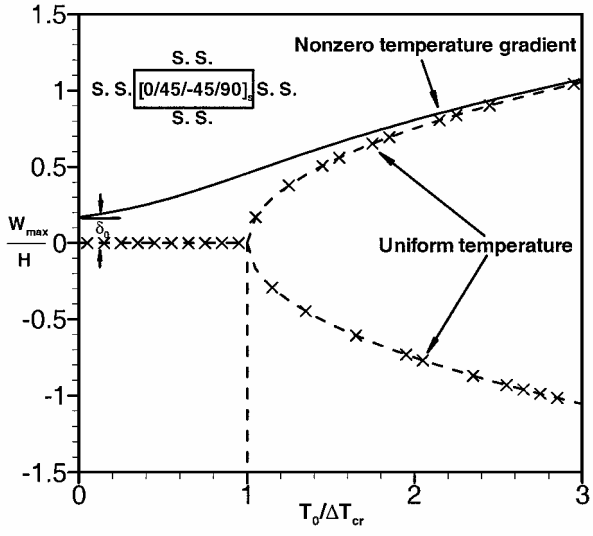

Fig. 8 Deflection characteristics of plate with/without temperature gradient.

the stability boundaries of higher damped panels. The case of a flow angle $\Lambda = 45$ deg is utilized, and the stability boundaries for $C_a = 0.01$, 0.05, and 0.1 are compared in Fig. 7. It is seen from Fig. 7 that when aerodynamic damping is high enough those ripples representing low stability boundaries disappear. The possible explanation is that higher aerodynamic damping makes flutter of thermally buckled plate less possible.

Flutter of Plates with Temperature Gradients

A temperature gradient introduces thermal bending moments to the plate that causes bending. Figure 8 shows the maximum deflections of a plate with and without a temperature gradient across the thickness (no aerodynamic effects involved). In Fig. 8 δ_0 represents the residual bending induced by thermal moment while the average temperature $T_0 = 0.0$. The solid line, defined as a primary branch by Shi et al.,[17] unlike the uniform temperature case has no symmetric bifurcation branches. It is known that for unsymmetrically laminated plates ($[B] \neq 0$) the primary branch appears even if the plate is heated uniformly (no residual bending deflection).

The stability boundaries of composite plates with simply supported edges experiencing nonzero temperature gradients across the plate thickness are studied in detail. Zero/nonzero flow angles and various average temperatures T_0 are considered, taking the critical buckling temperature ($\Delta T_{cr} = 13.737$°F or 7.63°C) of the simply supported plate as reference. The variation of stability boundaries is plotted in Fig. 9.

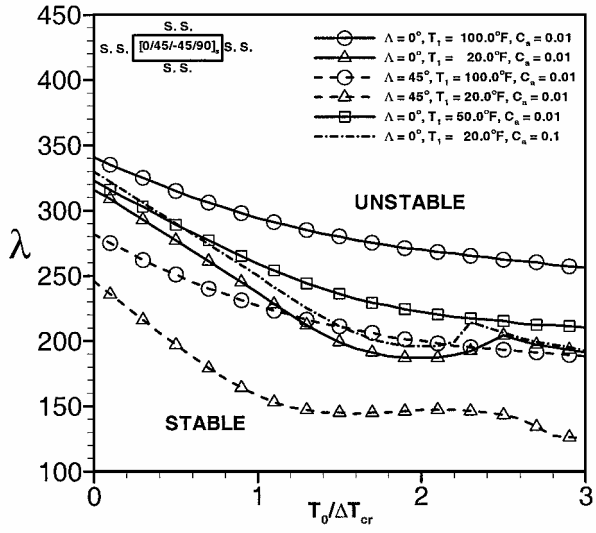

Fig. 9 Effects of temperature gradients on stability boundary of simply supported [0/45/−45/90]$_s$ rectangular plate.

The range of temperature gradients, which is typical for aerospace vehicles, is obtained from Refs. 20 and 29. Figure 9 reveals that 1) a nonzero flow angle results in destabilization of the plate, 2) an increasing temperature gradient enhances the stability boundary because large thermal moments result in large bending deflection that stiffens the plate, 3) as the average temperature T_0 increases the plate stiffness is softened and the stability boundary drops, and 4) for large temperature gradients the stability boundary is monotonously decreasing, but this is not true for the small gradient case. The possible explanation for this last point can be inferred from the interaction between stiffening caused by thermal bending induced by temperature gradient T_1 and softening caused by thermal expansion as a result of the effects of the average temperature (T_0 or $T_0/\Delta T_{cr}$). When T_1 is small, the bending of the plate is small. The expansion softening effects overwhelm the bending stiffening. As $T_0/\Delta T_{cr}$ increases, the softened plate is easier to deform so that stiffening effect from thermal moment is enlarged. This augmentation of stiffness might cancel the softening from thermal expansion and increase stability boundary locally. As $T_0/\Delta T_{cr}$ increases, softening caused by expansion will overwhelm stiffening again. However, for plates with large temperature gradients the plate experiences a significant bending for all cases. Additional flexibility brought by thermal expansion will not affect bending deflection. The interaction between softening and stiffening, for this case only, minimizes changes in the stability boundary, which can be concluded by comparing the curves for $\Lambda = 0$ deg, $T_1 = 11.11$°C (20.0°F), 27.78°C (50.0°F), and 55.56°C (100.0°F). The aerodynamic damping used for most of the curves is $C_a = 0.01$, except that the auxiliary curve ($\Lambda = 0$ deg, $T_1 = 11.11$°C) uses $C_a = 0.1$.

Conclusions

A finite element modal formulation to evaluate the combined effects of flow angle and elevated temperature on the stability boundary of supersonic panel flutter has been presented. Stability boundaries of both isotropic and composite plates are investigated.

For isotropic square plates heated uniformly, results show that flow angle has less influence on change of stability boundaries than temperature effects. But for composite plates flow angle effects on stability boundary cannot be ignored. Influence of aerodynamic damping on stability boundary is also studied. Although aerodynamic damping is small, thermally buckled composite plates may flutter at much lower dynamic pressure because frequency coalescence between modes other than the lowest two modes might occur.

It is found that for plates that experience temperature gradients across the thickness finite thermal deflections induced by thermal

moments will stiffen the plate and therefore enhance the stability boundary, whereas expansion of plates from elevated average temperatures will soften the plate. Interaction between the stiffening caused by temperature gradients and the softening caused by thermal expansion results in slowly decreasing stability boundary.

Acknowledgment

The first and third authors acknowledge the partial support by Grant NAG- 1-2150, NASA Langley Research Center.

References

[1]Korders, E. E., and Noll, R. B., "Theoretical Flutter Analysis of Flat Rectangular Panels in Uniform Coplanar with Arbitrary Direction," NASA TN D-1156, Jan. 1962.

[2]Bohon, H. L., "Flutter of Flat Rectangular Orthotropic Panels with Biaxial Loading and Arbitrary Flow Direction," NASA TN D-1949, Sept. 1963.

[3]Durvasula, S., "Flutter of Simply Supported, Parallelogrammic, Flat Panels in Supersonic Flow," *AIAA Journal*, Vol. 5, No. 9, 1967, pp. 1668–1673.

[4]Durvasula, S., "Flutter of Clamped Skew Panels in Supersonic Flow," *Journal of Aircraft*, Vol. 8, No. 6, 1971, pp. 461–466.

[5]Kariappa, Somashekar, B. R., and Shah, C. G., "Discrete Element Approach to Flutter of Skew Panels with In-Plane Forces under Yawed Supersonic Flow," *AIAA Journal*, Vol. 8, No. 11, 1970, pp. 2017–2022.

[6]Sander, G., Bon, C., and Geradin, M., "Finite Element Analysis of Supersonic Panel Flutter," *International Journal for Numerical Methods in Engineering*, Vol. 7, No. 3, 1973, pp. 379–394.

[7]Bismarck-Nasr, M. N., "Finite Element Analysis of Aeroelasticity of Plates and Shells," *Applied Mechanics Reviews*, Vol. 45, No. 12, Pt. 1, 1992, pp. 461–482.

[8]Mei, C., Abdel-Motagaly, K., and Chen, R., "Review of Nonlinear Panel Flutter at Supersonic and Hypersonic Speeds," *Applied Mechanics Reviews*, Vol. 52, No. 10, 1999, pp. 321–332.

[9]Shyprykevich, P., and Sawyer, J. W., "Orthotropic Panel Flutter at Arbitrary Yaw Angles-Experiment and Correlation with Theory," AIAA Paper 73-192, 11th Aerospace Sciences Meeting, Jan. 1973.

[10]Sawyer, J. W., "Flutter of Elastically Supported Orthotropic Panels Including the Effects of Flow Angle," NASA TN D-7491, May 1974.

[11]Houboult, J. C., "A Study of Several Aerothermoelastic Problems of Aircraft Structures in High-Speed Flight," Ph.D. Dissertation, Eidenössischen Technischen Hochschule, Swiss Federal Inst. of Technology, Zurich, Switzerland, 1958.

[12]Yang, T. Y., and Han, A. D., "Flutter of Thermally Buckled Finite Element Panels," *AIAA Journal*, Vol. 14, No. 7, 1976, pp. 975–977.

[13]Xue, D. Y., and Mei, C., "Finite Element Nonlinear Flutter and Fatigue Life of Two-Dimensional Panels with Temperature Effects," *Journal of Aircraft*, Vol. 30, No. 6, 1993, pp. 993–1000.

[14]Xue, D. Y., and Mei, C., "Finite Element Nonlinear Panel Flutter with Arbitrary Temperatures in Supersonic Flow," *AIAA Journal*, Vol. 31, No. 1, 1993, pp. 154–162.

[15]Liaw, D. G., "Nonlinear Supersonic Flutter of Laminated Composite Plates Under Thermal Loads," *Computers and Structures*, Vol. 65, No. 5, 1997, pp. 733–740.

[16]Abdel-Motaglay, K., Chen, R., and Mei, C., "Nonlinear Flutter of Composite Panels Under Yawed Supersonic Flow Using Finite Elements," *AIAA Journal*, Vol. 37, No. 9, 1999, pp. 1025–1032.

[17]Shi, Y., Lee, R. Y. Y., and Mei, C., "Thermal Postbuckling of Composite Plates Using the Finite Element Modal Coordinate Method," *Journal of Thermal Stresses*, Vol. 22, No. 6, 1999, pp. 595–614.

[18]Zhou, R. C., Xue D. Y., and Mei, C., "Finite Element Time Domain-Modal Formulation for Nonlinear Flutter of Composite Panels," *AIAA Journal*, Vol. 32, No. 10, 1994, pp. 2044–2052.

[19]Lee, J., "Large-Amplitude Plate Vibration in an Elevated Thermal Environment," *Applied Mechanics Reviews*, Vol. 46, No. 11, Pt. 2, 1993, pp. S242–S254.

[20]Moorthy, J., "Numerical Simulation of the Nonlinear Response of Composite Plates Under Combined Thermal and Acoustic Loading," Ph.D. Dissertation, Dept. of Aerospace Engineering, Old Dominion Univ., Norfolk, VA, Dec. 1994.

[21]Dowell, E. H., "Panel Flutter: A Review of the Aeroelastic Stability of Plates and Shells," *AIAA Journal*, Vol. 8, No. 3, 1970, pp. 385–399.

[22]Ashley, H., and Zartarian, G., "Piston Theory—A New Aerodynamic Tool for the Aeroelastician," *Journal of Aeronautical Science*, Vol. 23, No. 10, 1956, pp. 1109–1118.

[23]Dowell, E. H., "Nonlinear Oscillations of a Fluttering Plate," *AIAA Journal*, Vol. 4, No. 7, 1966, pp. 1267–1275.

[24]Xue, D. Y., "Finite Element Frequency Domain Solution of Nonlinear Panel Flutter with Temperature Effects and Fatigue Life Analysis," Ph.D. Dissertation, Dept. of Mechanical Engineering and Mechancis, Old Dominion Univ., Norfolk, VA, Oct. 1991.

[25]Bergan, P. G., and Clough, R. W., "Convergence Criteria for Iterative Process," *AIAA Journal*, Vol. 10, No. 8, 1972, pp. 1107, 1108.

[26]Weiliang, Y., and Dowell, E., "Limit Cycle Oscillation of a Fluttering Cantilever Plate," *AIAA Journal*, Vol. 29, No. 11, 1991, pp. 1929–1936.

[27]Lee, I., Lee, D.-M., and Oh, I.-K., "Supersonic Flutter Analysis of Stiffened Laminated Plates Subject to Thermal Load," *Journal of Sound and Vibration*, Vol. 224, No. 1, 1999, pp. 49–67.

[28]Paul, D. B., "Large Deflection of Clamped Rectangular Plates with Arbitrary Temperature Distributions," U.S. Air Force Wright Aeronautical Lab., AFWAL-TR-81-3003, Vol. 1, Wright–Patterson AFB, OH, Feb. 1982.

[29]Thornton, E. A., *Thermal Structures for Aerospace Applications*, AIAA Education Series, AIAA, Reston, VA, 1996, p. 88.